

# Competing phases in the extended U-V-J Hubbard model near the van Hove fillings

A.P. Kampf<sup>a</sup> and A.A. Katanin<sup>a,b</sup>

<sup>a</sup> *Institut für Physik, Theoretische Physik III,  
Elektronische Korrelationen und Magnetismus,  
Universität Augsburg, 86135 Augsburg, Germany*

<sup>b</sup> *Institute of Metal Physics, 620219 Ekaterinburg, Russia*

## Abstract

The phase diagram of the two-dimensional extended one-band  $U$ - $V$ - $J$  Hubbard model is considered within a mean-field approximation and two- and many-patch renormalization group (RG) approaches near the van Hove band fillings. While charge- and spin-flux phases are not stable at the mean-field level, they are identified as possible ground states in some parameter range within the RG treatment. We argue that in the physically relevant parameter range there is a complex competition between a spin-density wave, charge flux phases, and  $d$ -wave superconductivity.

PACS numbers: 71.10.Fd; 71.27.+a; 74.25.Dw

## I. INTRODUCTION

Despite many years of research the mysterious properties of underdoped high-temperature superconductors remain an unsolved and most challenging problem of strongly correlated electron physics. Recent theoretical proposals as well as experimental data trace the possible origin of the unconventional electronic properties of underdoped cuprates to a delicate competition between various types of ordering phenomena. Since metallic cuprates result from doping Mott-Hubbard antiferromagnetic insulators, it is natural that strong magnetic correlations persist for superconducting compositions but alternative ordering tendencies may be hidden as well.

The relation between superconductivity and antiferromagnetism and the attempt to treat both types of order on the same footing was the basis of the phenomenological SO(5) theory as originally proposed by Zhang [1]. Yet, the observation of inhomogeneous charge and spin structures in static stripe patterns in rare-earth doped  $\text{La}_{2-x}\text{Sr}_x\text{CuO}_4$  [2] and the appearance of an anisotropic *d*-wave like pseudogap at temperatures well above the superconducting transition have pointed to the possibility of nearby instabilities towards other phases in competition or coexistence with *d*-wave superconductivity.

The relevance of stripe patterns was proposed early on (for a review see, e.g., Ref. [3]), and years later their existence was indeed experimentally verified in  $\text{La}_{2-x-y}\text{Nd}_y\text{Sr}_x\text{CuO}_4$  [2]. These static stripe structures may in fact result from the lattice anisotropy connected to the  $\text{CuO}_6$  octahedral tilt pattern in the LTT phase of this compound [4]. Time-reversal symmetry breaking charge-flux (CF) [5–7] and spin-flux (SF, spin nematic) [8–10] phases were also proposed early on as possible ground states of the basic correlated electron Hamiltonians commonly used to model high- $T_c$  superconductors.

The idea of circulating orbital currents (also called an orbital antiferromagnet state [5]) was recently revived as the underlying origin of the pseudogap phase in underdoped cuprates [11]. Two variants of orbital current structures are currently discussed: Varma [12] proposed a circulating current pattern in the  $\text{CuO}_2$  planes which preserves the discrete translational

symmetry of the lattice, while the more recently proposed *d*-density wave (DDW) state [11,13] contains a staggered current pattern which doubles the unit cell. The latter state is in fact equivalent to the orbital antiferromagnet discussed a long time ago [6]. These time reversal symmetry breaking phases may furthermore coexist with *d*-wave superconductivity. Yet, another instability connected to the spontaneous deformation of the Fermi surface (Pomeranchuk instability, PI) was recently proposed for the two-dimensional Hubbard model [14]. It appears tempting to suggest a possible relation between the Pomeranchuk instability and stripe pattern formation.

Remarkably, the possible existence of orbital currents has most recently received experimental support. Angular-resolved photoemission with circularly polarized light identified intensity differences for left and right circularly polarized photons below the pseudogap temperature in Bi2212 [15] and c-axis oriented ordered magnetic moments were detected by spin-polarized neutron scattering in YBCO [16]. Both data sets can find a natural interpretation in terms of planar circulating current phases.

The tendency towards the formation of charge flux phases is most likely beyond the physics of the standard Hubbard model. In order to allow for a larger variety of competing or coexisting phases it appears therefore demanding to explore some extensions of the Hubbard model. A natural choice is to consider the extended *U-V-J* Hubbard model (*V* is a nearest-neighbor interaction and *J* is the Heisenberg exchange coupling). This model was chosen early on to study orbital antiferromagnetism and spin nematic phases. In one dimension (1D), this model was studied within the bosonization technique [17,18]. However, in 1D, one can not explore the possibility of charge- and spin-flux phases, but they were later on investigated in an extension to ladder systems [19]. In two dimensions, the *U-V-J* model was considered within mean-field approximation for *J* = 0 [20,21] and for *V* = 0 [22]. The possible coexistence of antiferromagnetism and *d*-wave superconductivity [23], and charge flux and *d*-wave superconductivity [24] was discussed in this context. More recently, the possibility of coexisting phases was reanalyzed within a mean-field treatment of the extended Hubbard model which furthermore includes correlated hopping [25].

Common to these studies is the need to go beyond the standard one-band Hubbard model to allow for a variety of alternative ordering phenomena. However, a mean-field treatment does not allow for an accurate treatment of fluctuations which may alter the complex ground-state phase diagram. Other analytical and numerical methods are needed for a reliable insight into the interplay of various types of ordering tendencies. One possible step forward in this direction has been the recent analysis of competing phases within dynamical mean-field theory [26].

Another possible route is to start from the weak-coupling regime, where magnetic or superconducting instabilities can result from nesting of the Fermi surface (FS) or van Hove singularities (vHS) in the density of states. The latter case is also relevant from a material oriented point of view since the FS of cuprates in an intermediate doping regime is close to vHS of the electron spectrum [27–29]. Schulz considered [30] different phases near van Hove band fillings within a mean-field-like analysis which, however, did not take into account the interplay of different electron scattering channels. The parquet approach was first applied to the extended Hubbard model with a nearest-neighbor hopping in Refs. [31–33], where besides the standard superconducting, spin- and charge-density-wave instabilities, the possibilities for spin- and charge-flux instabilities were also discussed. Recently, the standard Hubbard model ( $V = J = 0$ ) was investigated within the renormalization-group (RG) approach on a patched FS using the Polchinsky flow equations [34], Wick-ordered RG equations [35], and a RG scheme for one-particle irreducible functions [36]. The possibility of the charge-flux phase as well as the Pomeranchuk instability for the standard Hubbard model was addressed in Ref. [37]. These latter methods have the advantage that they allow to take into account the contributions of the entire FS. At the same time, even the restriction of the momenta to the vicinity of van Hove points (the so called “two-patch” approach originally proposed in Refs. [38,39]) can capture already the essential physics and can give results which are in qualitative agreement with the RG approaches on patched Fermi surfaces, see Ref. [40]. This two-patch approach allows to include the contribution of particle-hole scattering at small momenta which is expected to be important for the determination of the complete ground-

state phase diagram. The role of this type of scattering was also explored within the RG approach with a temperature cutoff on the patched FS [41]. Although the phase diagram of the  $U$ - $V$ - $J$  Hubbard model was investigated previously within the two-patch RG approach, only the cases of  $J = 0$  [21] and arbitrary  $J$  with nearest-neighbor hopping dispersion [42], but without the contribution of the small-momenta particle-hole scattering were considered. The same model within the many-patch approach was not systematically studied so far.

In this paper we reconsider the phase diagram of the extended  $U$ - $V$ - $J$  Hubbard model with special emphasis on the possibility of flux phases. We employ the mean-field approximation, two- and many-patch RG approaches. The paper is organized as follows: In Sect. II we start with the mean-field phase diagram of the  $U$ - $V$ - $J$  Hubbard model. In Sect. III we describe the two- and many-patch RG schemes and compare the results obtained with both approaches to the mean-field phase diagram. In Sect. IV we complement the RG analysis by symmetry arguments. Finally, in Sect. V we summarize the main results and conclude.

## II. MEAN-FIELD ANALYSIS

We consider the extended  $U$ - $V$ - $J$  Hubbard model on a square lattice as given by

$$H = - \sum_{ij\sigma} t_{ij} c_{i\sigma}^\dagger c_{j\sigma} + U \sum_i n_{i\uparrow} n_{i\downarrow} + \frac{V}{2} \sum_{\langle ij \rangle} n_i n_j + \frac{J}{2} \sum_{\langle ij \rangle} \mathbf{S}_i \cdot \mathbf{S}_j - \mu N_e \quad (1)$$

where the hopping amplitude  $t_{ij} = t$  for nearest neighbor sites  $i$  and  $j$  and  $t_{ij} = -t'$  for next-nearest neighbor sites ( $t, t' > 0$ );  $N_e$  is the total number of electrons.  $U > 0$  is the on-site and  $V$  the nearest-neighbor interaction,  $J$  is the Heisenberg exchange coupling, and

$$n_i = \sum_{\sigma} c_{i\sigma}^\dagger c_{i\sigma}, \quad \mathbf{S}_i = \frac{1}{2} \sum_{\sigma\sigma'} c_{i\sigma}^\dagger \boldsymbol{\sigma}_{\sigma\sigma'} c_{i\sigma'};$$

$\boldsymbol{\sigma}_{\sigma\sigma'}$  are the Pauli matrices. We introduce operators which correspond to different types of order

$$\hat{O}_{\text{CDW}}(i) = \frac{1}{2}(-1)^i \sum_{\sigma} (c_{i\sigma}^\dagger c_{i\sigma} - n/2),$$

$$\begin{aligned}
\hat{O}_{\text{SDW}}(i) &= \frac{1}{2}(-1)^i \sum_{\sigma} \sigma (c_{i\sigma}^{\dagger} c_{i\sigma} - n/2), \\
\hat{O}_{\text{dSC}}(i) &= \frac{1}{2z} \sum_{j\sigma} \lambda_{ij} \sigma c_{i\sigma}^{\dagger} c_{j,-\sigma}^{\dagger}, \\
\hat{O}_{\text{CF}}(i) &= -\frac{i}{2z} (-1)^i \sum_{j\sigma} \lambda_{ij} c_{i\sigma}^{\dagger} c_{j\sigma}, \\
\hat{O}_{\text{SF}}(i) &= -\frac{i}{2z} (-1)^i \sum_{j\sigma} \lambda_{ij} \sigma c_{i\sigma}^{\dagger} c_{j\sigma}, \\
\hat{O}_{\text{F}}(i) &= \frac{1}{2} \sum_{\sigma} \sigma (c_{i\sigma}^{\dagger} c_{i\sigma} - 1/2),
\end{aligned} \tag{2}$$

where  $\lambda_{ij} = +1$  ( $-1$ ) for  $j = i + \delta_x(\delta_y)$  and zero otherwise;  $\delta_{x,y}$  denote unit vectors which connect to nearest neighbor sites in  $x$  and  $y$  directions respectively.  $(-1)^i \equiv (-1)^{i_x+i_y}$ ,  $z = 4$  is the number of nearest neighbor sites on the square lattice, and  $n$  is the electron density. Nonzero average values of the operators  $\hat{O}_{\text{CDW}}(i)$  and  $\hat{O}_{\text{SDW}}(i)$  correspond to charge- and spin density wave states,  $\hat{O}_{\text{dSC}}(i)$  to  $d$ -wave superconductivity,  $\hat{O}_{\text{CF}}$  and  $\hat{O}_{\text{SF}}$  to states with charge flux (the orbital antiferromagnet state) [5,6,13] or spin flux (spin nematic state) [8–10], respectively, and finally  $\hat{O}_{\text{F}}$  corresponds to a ferromagnetic state. We decouple the interactions by introducing the order parameters  $O_m = \langle \hat{O}_m \rangle$  ( $m = \text{CDW, SDW, ...}$ ), and arrive at the mean-field Hamiltonian

$$H = \sum_{\mathbf{k}\sigma} \varepsilon_{\mathbf{k}} c_{\mathbf{k}\sigma}^{\dagger} c_{\mathbf{k}\sigma} + \sum_{\mathbf{k}} \Delta_m \hat{O}_m(\mathbf{k}) + \frac{\Delta_m^2}{\Gamma_m} \tag{3}$$

where

$$\varepsilon_{\mathbf{k}} = -2t(\cos k_x + \cos k_y) + 4t' \cos k_x \cos k_y - \mu. \tag{4}$$

$\hat{O}_m(\mathbf{k})$  are the Fourier transforms of the operators in Eq. (2),  $\Delta_m = O_m \Gamma_m$  and

$$\begin{aligned}
\Gamma_{\text{CDW}} &= 8V - U; \quad \Gamma_{\text{SDW}} = U + 2J; \quad \Gamma_{\text{dSC}} = 3J - 4V; \\
\Gamma_{\text{CF}} &= 3J + 4V; \quad \Gamma_{\text{SF}} = 4V - J; \quad \Gamma_{\text{F}} = U - 2J.
\end{aligned} \tag{5}$$

At finite temperature  $T$  the self-consistency conditions lead to the mean-field equations (see e.g. Ref. [8])

$$\begin{aligned}
1 &= \frac{\Gamma_m}{2N} \sum'_{\mathbf{k}, \alpha=\pm} \frac{\phi_{\mathbf{k}}^2}{E_{\mathbf{k}\alpha}^i} \tanh \frac{E_{\mathbf{k}\alpha}^m}{2T}, \\
n &= 1 - \frac{1}{2N} \sum'_{\mathbf{k}, \alpha=\pm} \tanh \frac{E_{\mathbf{k}\alpha}^m}{2T},
\end{aligned} \tag{6}$$

where  $\Sigma'$  denotes the summation over momenta in the magnetic Brillouin zone defined by  $\cos k_x + \cos k_y \geq 0$  (the lattice constant has been set to unity);  $\phi_{\mathbf{k}} = 1$  for SDW and CDW phases and  $\phi_{\mathbf{k}} = f_{\mathbf{k}} \equiv (\cos k_x - \cos k_y)/2$  for CF, SF, and dSC phases,

$$E_{\mathbf{k}\alpha}^m = \frac{\varepsilon_{\mathbf{k}} + \varepsilon_{\mathbf{k}+\mathbf{Q}}}{2} + \frac{\alpha}{2} \sqrt{(\varepsilon_{\mathbf{k}} - \varepsilon_{\mathbf{k}+\mathbf{Q}})^2 + 4\phi_{\mathbf{k}}^2 \Delta_m^2} \tag{7}$$

for  $m = \text{SDW, CDW, CF or SF}$  and

$$E_{\mathbf{k}\alpha}^{\text{dSC}} = \frac{1}{2} \sqrt{(\varepsilon_{\mathbf{k}} - \varepsilon_{\mathbf{k}+\mathbf{Q}})^2 + 4\phi_{\mathbf{k}}^2 \Delta_{\text{dSC}}^2}. \tag{8}$$

$\mathbf{Q} = (\pi, \pi)$  is the wavevector for staggered order. For the ferromagnetic phase the mean-field equations read

$$\begin{aligned}
\Delta_{\text{F}} &= \frac{\Gamma_{\text{F}}}{N} \sum_{\mathbf{k}, \alpha=\pm} \alpha f_{\mathbf{k}\alpha}, \quad n = \frac{1}{N} \sum_{\mathbf{k}\alpha} f_{\mathbf{k}\alpha}, \\
E_{\mathbf{k}\alpha}^{\text{F}} &= \varepsilon_{\mathbf{k}} - \alpha \Delta_{\text{F}}
\end{aligned} \tag{9}$$

where  $f_{\mathbf{k}\alpha} \equiv f(E_{\mathbf{k}\alpha}^{\text{F}})$  is the Fermi function. Non-trivial mean-field solutions exist only for  $\Gamma_m > 0$ , which therefore determines the borders of absolute stability of the corresponding phases in the phase diagram.

We also allow for coexistence of antiferromagnetism,  $d$ -wave superconductivity, and charge-flux phases. The corresponding MF equations are the generalization of those for the coexistence of SDW and dSC phases [23] and CF and dSC phases [24], and have the form

$$\begin{aligned}
1 &= \frac{\Gamma_{\text{SDW}}}{2N} \sum'_{\mathbf{k}, \alpha=\pm} \frac{1}{E_{\mathbf{k}\alpha}} \tanh \frac{E_{\mathbf{k}\alpha}}{2T} \left( 1 + \frac{\varepsilon_{\mathbf{k}} + \varepsilon_{\mathbf{k}+\mathbf{Q}}}{g_{k\alpha}} \right), \\
1 &= \frac{\Gamma_{\text{dSC}}}{2N} \sum'_{\mathbf{k}, \alpha=\pm} \frac{f_{\mathbf{k}}^2}{E_{\mathbf{k}\alpha}} \tanh \frac{E_{\mathbf{k}\alpha}}{2T},
\end{aligned}$$

$$1 = \frac{\Gamma_{\text{CF}}}{2N} \sum'_{\mathbf{k}, \alpha=\pm} \frac{f_{\mathbf{k}}^2}{E_{\mathbf{k}\alpha}} \tanh \frac{E_{\mathbf{k}\alpha}}{2T} \left( 1 + \frac{\varepsilon_{\mathbf{k}} + \varepsilon_{\mathbf{k}+\mathbf{Q}}}{g_{k\alpha}} \right),$$

$$n = 1 - \frac{1}{2N} \sum'_{\mathbf{k}, \alpha=\pm} \frac{1}{E_{\mathbf{k}\alpha}} \tanh \frac{E_{\mathbf{k}\alpha}}{2T} (\varepsilon_{\mathbf{k}} + \varepsilon_{\mathbf{k}+\mathbf{Q}} + g_{k\alpha}), \quad (10)$$

where the electronic spectrum is given by

$$E_{\mathbf{k}\alpha} = \sqrt{(\varepsilon_{\mathbf{k}}^2 + \varepsilon_{\mathbf{k}+\mathbf{Q}}^2)/2 + \Delta_{\text{SDW}}^2 + f_{\mathbf{k}}^2(\Delta_{\text{CF}}^2 + \Delta_{\text{dSC}}^2) + (\varepsilon_{\mathbf{k}} + \varepsilon_{\mathbf{k}+\mathbf{Q}})g_{k\alpha}/2},$$

$$g_{\mathbf{k}\alpha} = \alpha \sqrt{(\varepsilon_{\mathbf{k}} - \varepsilon_{\mathbf{k}+\mathbf{Q}})^2 + 4(\Delta_{\text{SDW}}^2 + f_{\mathbf{k}}^2\Delta_{\text{dSC}}^2)}. \quad (11)$$

We note that a nonzero expectation value of both, antiferromagnetic and superconducting order parameters, produces also a nonzero  $\pi$ -triplet pairing amplitude with momentum  $\mathbf{Q}$  (see e.g. Ref. [23]). Analogously nonzero values of charge flux and  $d$ -wave superconducting order parameters lead to a finite singlet pairing amplitude with momentum  $\mathbf{Q}$  (so called  $\eta$ -pairing). Here, we do not include  $\pi$ - and  $\eta$ -pairing in the mean-field analysis, since it was verified numerically [23] that the corresponding amplitudes are significantly smaller than the amplitudes of the corresponding “parent” order parameters.

The mean-field equations (6), (9), and (10) were solved numerically for  $T = 0$ ,  $U = 4t$ ,  $t' = 0.1t$ , and band filling  $n = 0.92$  (which is the van Hove filling for this value of  $t'/t$ , see the next section). Since the regions of stability of different phases overlap, we compare the energies  $E = \langle H \rangle + \mu N_e$  to identify the mean-field ground state. The resulting phase diagram is shown in Fig. 1. At positive  $J$  and not too large  $V$  we find coexistence of a spin density wave with  $d$ -wave superconductivity. However, the fraction of superconductivity in this phase is quite small (for  $V = 0$ ,  $J = 0.5U$  we have  $O_{\text{SDW}} = 0.40$  and  $O_{\text{dSC}} = 0.06$ ). With decreasing  $V$  the superconducting fraction increases and becomes substantial close to the transition into the pure dSC state (for  $V = -3U/4$ ,  $J = -0.05U$  we have  $O_{\text{SDW}} = 0.18$  and  $O_{\text{dSC}} = 0.12$ ), and finally at the boundary between the dSC and SDW+dSC phases the antiferromagnetic order parameter vanishes continuously. Therefore, this transition as well as the transition from the SDW into the SDW+dSC phase is of second order. All other phase boundary lines in Fig. 1 correspond to first order transitions. The CF, SF, and CF+dSC

phases are not energetically favorable at all on the mean-field level, the dSC phase is stable only for  $V < -2t$ . The mean-field phase diagram at other fillings or other  $t'/t$  is similar. In the special case  $t' = 0$  and half-filling, the coexistence region of the SDW+dSC phase is replaced by a pure SDW state.

Away from half-filling the phases with ordering wavevector  $\mathbf{Q} = (\pi, \pi)$ , i.e. CDW, SDW, CF, and SF phases are usually unstable towards phase separation (see e.g. the discussion in Refs. [43,44]). To analyze this possibility, we calculate the isothermal compressibility  $\kappa_T$  defined by

$$\kappa_T = \frac{1}{n^2} \frac{\partial n}{\partial \mu} = \frac{N}{n^2} \left( \frac{\partial^2 E}{\partial n^2} \right)^{-1}. \quad (12)$$

A negative  $\kappa_T$  necessarily implies the thermodynamic instability of the considered homogeneous phase and a possible tendency towards phase separation. The numerical analysis shows that all above phases are indeed unstable except for the SDW+dSC phase in the region  $J \ll U$  and  $V \rightarrow -U$  where the fraction of the SDW order parameter is small.

The above mean-field results provide a rough qualitative picture for the regions of different stable phases in the ground-state phase diagram of the  $U$ - $V$ - $J$  Hubbard model. More detailed information is extracted from the weak-coupling RG treatments discussed below.

### III. RENORMALIZATION-GROUP ANALYSIS

#### A. Two-patch analysis

The tight-binding spectrum (4) leads to vHS in the density of states arising from the contributions of the points  $\mathbf{k}_A = (\pi, 0)$  and  $\mathbf{k}_B = (0, \pi)$ . These singularities lie at the FS if  $\mu = -4t'$ . For  $t' = 0$  the corresponding filling is  $n_{VH} = 1$  and the FS is nested, but the nesting is removed for  $t'/t > 0$ , when  $n_{VH} < 1$ . The shape of the FS at different  $t'/t$  and van Hove band fillings is shown in Fig. 2.

The two-patch approach [38–40] considers the fillings which are close to the van Hove band fillings. At these fillings the density of states at the Fermi energy and the electron-

electron interaction vertices at momenta  $\mathbf{k} = \mathbf{k}_{A,B}$  contain logarithmical divergencies coming from the momentum integrations in the vicinity of the points  $\mathbf{k} = \mathbf{k}_{A,B}$ , and therefore one can expect that the contributions from the vicinities of these points are the most important for the calculation of the renormalized electron-electron interaction vertices.

We start by rewriting the  $U-V-J$  Hamiltonian in momentum space

$$H = \sum_{\mathbf{k}\sigma} \varepsilon_{\mathbf{k}} c_{\mathbf{k}\sigma}^\dagger c_{\mathbf{k}\sigma} + \frac{1}{2N^2} \sum_{\mathbf{k}_1 \mathbf{k}_2 \mathbf{k}_3 \mathbf{k}_4} \sum_{\sigma\sigma'} g(\mathbf{k}_1, \mathbf{k}_2, \mathbf{k}_3, \mathbf{k}_4) c_{\mathbf{k}_1\sigma}^\dagger c_{\mathbf{k}_2\sigma'}^\dagger c_{\mathbf{k}_3\sigma'} c_{\mathbf{k}_4\sigma} \delta_{\mathbf{k}_1 + \mathbf{k}_2 - \mathbf{k}_3 - \mathbf{k}_4} \quad (13)$$

where

$$g(\mathbf{k}_1, \mathbf{k}_2, \mathbf{k}_3, \mathbf{k}_4) = U + (V - J/4)\gamma_{\mathbf{k}_2 - \mathbf{k}_3} - (J/2)\gamma_{\mathbf{k}_3 - \mathbf{k}_1} \quad (14)$$

$\gamma_{\mathbf{k}} = 2(\cos k_x + \cos k_y)$  and the Kronecker  $\delta$ -symbol ensures momentum conservation. Since we restrict the momenta to the vicinity of  $\mathbf{k}_A$  and  $\mathbf{k}_B$ , it is convenient to introduce new electron operators  $a_{\mathbf{k}}$  and  $b_{\mathbf{k}}$  by

$$c_{\mathbf{k}\sigma} = \begin{cases} a_{\mathbf{k}-\mathbf{k}_A, \sigma} & \mathbf{k} \in O(A) \\ b_{\mathbf{k}-\mathbf{k}_B, \sigma} & \mathbf{k} \in O(B) \end{cases}$$

here  $O(A) = \{\mathbf{k} : |\mathbf{k} - \mathbf{k}_A| < \Lambda\}$  and similar for  $B$ ;  $\Lambda$  is a momentum cutoff parameter. We expand the spectrum near the van Hove points

$$\begin{aligned} \varepsilon_{\mathbf{k}_A + \mathbf{p}} \equiv \varepsilon_{\mathbf{p}}^A &= -2t(\sin^2 \varphi p_x^2 - \cos^2 \varphi p_y^2) - \tilde{\mu} \\ &= -2tp_+ p_- - \tilde{\mu} \end{aligned} \quad (15a)$$

$$\begin{aligned} \varepsilon_{\mathbf{k}_B + \mathbf{p}} \equiv \varepsilon_{\mathbf{p}}^B &= 2t(\cos^2 \varphi p_x^2 - \sin^2 \varphi p_y^2) - \tilde{\mu} \\ &= 2t\tilde{p}_+ \tilde{p}_- - \tilde{\mu} \end{aligned} \quad (15b)$$

where  $\cos(2\varphi) = R = 2t'/t$ ,  $\tilde{\mu} = \mu + 4t'$ ,  $p_{\pm} = p_x \sin \varphi \pm p_y \cos \varphi$ ,  $\tilde{p}_{\pm} = p_x \sin \varphi \pm p_y \cos \varphi$  and rewrite the Hamiltonian in the form

$$\begin{aligned} H &= \sum_{\mathbf{p}\sigma} \varepsilon_{\mathbf{p}}^A a_{\mathbf{p}\sigma}^\dagger a_{\mathbf{p}\sigma} + \sum_{\mathbf{p}\sigma} \varepsilon_{\mathbf{p}}^B b_{\mathbf{p}\sigma}^\dagger b_{\mathbf{p}\sigma} \\ &+ \frac{2\pi^2 t}{N^2} \sum_{\mathbf{p}_i, \sigma\sigma'} [g_1(\lambda) a_{\mathbf{p}_1\sigma}^\dagger b_{\mathbf{p}_2\sigma'}^\dagger a_{\mathbf{p}_3\sigma'} b_{\mathbf{p}_4\sigma} + g_2(\lambda) a_{\mathbf{p}_1\sigma}^\dagger b_{\mathbf{p}_2\sigma'}^\dagger b_{\mathbf{p}_3\sigma'} a_{\mathbf{p}_4\sigma}] \delta_{\mathbf{p}_1 + \mathbf{p}_2 - \mathbf{p}_3 - \mathbf{p}_4} \\ &+ \frac{\pi^2 t}{N^2} \sum_{\mathbf{p}_i, \sigma\sigma'} [g_3(\lambda) a_{\mathbf{p}_1\sigma}^\dagger a_{\mathbf{p}_2\sigma'}^\dagger b_{\mathbf{p}_3\sigma'} b_{\mathbf{p}_4\sigma} + g_4(\lambda) a_{\mathbf{p}_1\sigma}^\dagger a_{\mathbf{p}_2\sigma'}^\dagger a_{\mathbf{p}_3\sigma'} a_{\mathbf{p}_4\sigma} + a \leftrightarrow b] \delta_{\mathbf{p}_1 + \mathbf{p}_2 - \mathbf{p}_3 - \mathbf{p}_4} \end{aligned} \quad (16)$$

where  $\varepsilon_{\mathbf{p}}^{A,B} = \varepsilon_{\mathbf{k}_{A,B}+\mathbf{p}}$ ,  $\lambda = \ln(\Lambda/\max(p_{i+}, p_{i-}, \tilde{p}_{i+}, \tilde{p}_{i-}, |\mu|/t))$ ; the summation is restricted to momenta  $|\mathbf{p}_i| < \Lambda$ . Neglecting the weak (non-logarithmical) dependence of the vertices  $g_i$  on momenta at  $|\mathbf{p}_i| < \Lambda$ , we obtain the bare values of the vertices  $g_i^0$  which are independent of  $\lambda$  and given by

$$\begin{aligned} g_1^0 &= g(\mathbf{k}_A, \mathbf{k}_B, \mathbf{k}_A, \mathbf{k}_B) = g_0(1 - 4V/U - J/U), \\ g_2^0 &= g(\mathbf{k}_A, \mathbf{k}_B, \mathbf{k}_B, \mathbf{k}_A) = g_0(1 + 4V/U + J/U), \\ g_3^0 &= g(\mathbf{k}_A, \mathbf{k}_A, \mathbf{k}_B, \mathbf{k}_B) = g_0(1 - 4V/U + 3J/U), \\ g_4^0 &= g(\mathbf{k}_A, \mathbf{k}_A, \mathbf{k}_A, \mathbf{k}_A) = g_0(1 + 4V/U - 3J/U). \end{aligned} \quad (17)$$

where  $g_0 = U/(4\pi^2 t)$  is the dimensionless coupling parameter. Note that at half filling and  $t' = 0$  the contributions of the flat, nested parts of the FS (which should be considered separately, see, e.g. Ref. [33] and references therein) is neglected. The contribution of these nested parts of the Fermi surface can be considered within the many-patch approach, as we discuss in the next section.

To obtain the dependence of the vertices  $g_i$  on  $\lambda$  we apply the RG analysis. We start with the bare values of the vertices at momenta far from van Hove singularities, i.e. with  $g_i^0$ , and integrate out the fermions  $a_{\mathbf{p}}$  with momenta  $\Lambda e^{-\lambda} < p_{\pm} < \Lambda e^{-\lambda-d\lambda}$  and fermions  $b_{\mathbf{p}}$  with momenta  $\Lambda e^{-\lambda} < \tilde{p}_{\pm} < \Lambda e^{-\lambda-d\lambda}$  at each RG step. We consider first the one-loop corrections which contain particle-hole ( $ph$ ) and particle-particle ( $pp$ ) bubbles at small momenta and momenta close to  $\mathbf{Q}$ . The results for these bubbles can be summarized as follows:

$$\Pi_{\mathbf{q}}^{pp} = \sum_{\Lambda e^{-\lambda} < p_{\pm} < \Lambda} \frac{1 - f(\varepsilon_{\mathbf{p}}^A) - f(\varepsilon_{\mathbf{p}+\mathbf{q}}^A)}{\varepsilon_{\mathbf{p}}^A + \varepsilon_{\mathbf{p}+\mathbf{q}}^A} = \frac{c_0}{4\pi^2 t} \lambda^2, \quad (18a)$$

$$\Pi_{\mathbf{q}+\mathbf{Q}}^{ph} = \sum_{\Lambda e^{-\lambda} < p_{\pm} < \Lambda} \frac{f(\varepsilon_{\mathbf{p}}^A) - f(\varepsilon_{\mathbf{p}+\mathbf{q}}^B)}{\varepsilon_{\mathbf{p}}^A - \varepsilon_{\mathbf{p}+\mathbf{q}}^B} = \frac{1}{4\pi^2 t} \min(\lambda^2, 2z_{\mathbf{Q}}), \quad (18b)$$

$$\Pi_{\mathbf{q}+\mathbf{Q}}^{pp} = \sum_{\Lambda e^{-\lambda} < p_{\pm} < \Lambda} \frac{1 - f(\varepsilon_{\mathbf{p}}^A) - f(\varepsilon_{\mathbf{p}+\mathbf{q}}^B)}{\varepsilon_{\mathbf{p}}^A + \varepsilon_{\mathbf{p}+\mathbf{q}}^B} = \frac{c_{\mathbf{Q}}}{2\pi^2 t} \lambda, \quad (18c)$$

where

$$c_0 = 1/\sin(2\varphi) = 1/\sqrt{1 - R^2},$$

$$c_{\mathbf{Q}} = \tan^{-1}(R/\sqrt{1-R^2})/R, \\ z_{\mathbf{Q}} = \ln[(1+\sqrt{1-R^2})/R]. \quad (19)$$

The contribution of the slices  $\Lambda e^{-\lambda} < p_{\pm}, \tilde{p}_{\pm} < \Lambda e^{-\lambda-d\lambda}$  is obtained by taking the derivatives  $d\Pi_i/d\lambda$ . Since the contribution to the particle-hole ( $\Pi_{\mathbf{q}}^{ph}$ ) channel is concentrated near the FS, we use the weaker cutoff condition  $\Lambda e^{-\lambda} < p_+ < \Lambda$  or  $\Lambda e^{-\lambda} < p_- < \Lambda$  for this channel which gives

$$\Pi_{\mathbf{q}}^{ph} = \sum_{\Lambda e^{-\lambda} < p_+ < \Lambda \text{ or } \Lambda e^{-\lambda} < p_- < \Lambda} \frac{f(\varepsilon_{\mathbf{p}}^A) - f(\varepsilon_{\mathbf{p}+\mathbf{q}}^A)}{\varepsilon_{\mathbf{p}}^A - \varepsilon_{\mathbf{p}+\mathbf{q}}^A} = \frac{z_0 \lambda}{2\pi^2 t} \quad (20)$$

with  $z_0 = c_0$ . A more accurate treatment of the  $ph$  channel requires the parquet summation of the one-loop diagrams, it was shown, however, in Ref. [40] that the corresponding corrections do not change qualitatively the results. Equation (20) can be justified also by considering the temperature flow of the vertices on a patched FS as proposed in Ref. [41] (see also the next section).

While the bubbles  $\Pi_{\mathbf{Q}}^{ph}$  (at  $\lambda < 2z_{\mathbf{Q}}$ ) and  $\Pi_0^{pp}$  contain squared logarithms, the bubbles  $\Pi_{\mathbf{Q}}^{ph}$  (at  $\lambda > 2z_{\mathbf{Q}}$ ),  $\Pi_0^{ph}$  and  $\Pi_{\mathbf{Q}}^{pp}$  contain only single-logarithmical divergencies. Strictly speaking, the RG approach does not perform a correct summation of these subleading divergencies. However, one can not simply neglect the single-logarithmical contributions ( $\Pi_{\mathbf{q}+\mathbf{Q}}^{pp}$  at  $\lambda < 2z_{\mathbf{Q}}$ ,  $\Pi_0^{ph}$  and  $\Pi_{\mathbf{q}}^{ph}$ ) in comparison to the squared-logarithmical ones, since it amounts to ignore some electron scattering channels and therefore would exclude the possibility of related orders, see Ref. [40] for a discussion. Mathematically, this difficulty manifests itself in the corresponding phases by the growing of the vertices which are multiplied by single logarithms, whose contribution can therefore become comparable to the squared-logarithmic contributions [40].

As we will see below from the solution of the RG equations, in the weak-coupling regime at small  $t'/t \ll 1$  the contribution of the subleading corrections  $\Pi_0^{ph}$  and  $\Pi_{\mathbf{Q}}^{pp}$  is small so that they do not change substantially the flow of the coupling constants. With increasing coupling, the contribution of single-logarithmical terms is comparable to the contribution

of the leading squared-logarithmical terms which reflects the possibility of a corresponding ordering phenomena (e.g. ferromagnetism) in the strong-coupling regime, although the latter can not be explored within the weak-coupling RG approach.

At intermediate  $t'/t$  the situation changes. In this case the contributions of different channels (containing single- and double-logarithmical terms) are comparable already in the weak-coupling regime. We have checked however, that even for intermediate  $t'/t$  the qualitative results of the two-patch RG approach do not depend on the cutoff procedure, which means that the treatment of the subleading single-logarithmical terms within the same RG procedure for intermediate  $t'/t$  is qualitatively reliable. Therefore, we take into account the contribution of both, single- and squared-logarithmical terms in Eqs. (18) and (20). At the same time, the contribution of the subleading single-logarithmical term in Eq. (18a) can be safely neglected, since it is multiplied by the same vertex as the leading one and therefore is always subleading.

We determine the RG equations for the vertices  $g_i(\lambda)$  in the form [38–40]

$$\begin{aligned} dg_1/d\lambda &= 2d_1(\lambda)g_1(g_2 - g_1) + 2d_2g_1g_4 - 2d_3g_1g_2, \\ dg_2/d\lambda &= d_1(\lambda)(g_2^2 + g_3^2) + 2d_2(g_1 - g_2)g_4 - d_3(g_1^2 + g_2^2), \\ dg_3/d\lambda &= -2d_0(\lambda)g_3g_4 + 2d_1(\lambda)g_3(2g_2 - g_1), \\ dg_4/d\lambda &= -d_0(\lambda)(g_3^2 + g_4^2) + d_2(g_1^2 + 2g_1g_2 - 2g_2^2 + g_4^2), \end{aligned} \quad (21)$$

where

$$\begin{aligned} d_0(\lambda) &= 2c_0\lambda, \quad d_2 = 2z_0; \quad d_3 = 2c_Q; \\ d_1(\lambda) &= 2 \min(\lambda, z_Q). \end{aligned} \quad (22)$$

Eqs. (21) have to be solved with the initial conditions  $g_i(1) = g_i^0$ . Note that we neglect here the renormalization of coupling constants which arise from non-logarithmical contributions at  $\lambda < 1$ , this renormalization is small provided that the condition  $g_i^0 \ll 1$  is satisfied.

Eqs. (21) coincide with the temperature cutoff RG approach for one-particle irreducible functions on the patched FS [41] (see Sect. IIIB) in the approximation that the vertex is

constant (i.e. does not depend on the patch) for the momenta in the vicinity of the vHS (for  $|\mathbf{p}_i| < \Lambda$ ) and zero far from it (when  $|\mathbf{p}_i| > \Lambda$  at least for one  $i = 1\dots 4$ ). Therefore, the real dependence of the vertices on the momenta along the FS is replaced by a step function in the two-patch approach. At the same time, the momentum dependence of the vertices in the direction perpendicular to the FS is treated correctly through the scaling variable  $\lambda$ . Note however, that the momentum dependence of the electronic spectrum within each patch is correctly taken into account in the two-patch approach.

Strictly speaking, some of the two-loop diagrams (e.g. the self-energy corrections) give contributions of the same order as the single-logarithmical terms which we treat here and they should be taken into account as well. However, the analysis of such contributions is rather involved and the subject for future work [45]. Note that this difficulty is also “hidden” in the RG approaches on a patched FS where additional logarithmical divergencies arise from the momentum integration along the FS.

In order to explore the possible instabilities of the system, we consider the behavior of the zero-frequency, time-ordered response functions at zero temperature

$$\chi_m(\mathbf{q}) = \int_{-\infty}^{\infty} d\tau \langle T [\hat{O}_m(\mathbf{q}, \tau) \hat{O}_m(-\mathbf{q}, 0)] \rangle \quad (23)$$

where  $\hat{O}_m(\mathbf{q}, \tau)$  denote the Fourier components of the operators (2) in the Heisenberg representation. Besides the operators in Eq. (2) we also test, following Refs. [21,42], the susceptibilities which correspond to the operators

$$\begin{aligned} \hat{Q}(i) &= \frac{1}{2} \sum_{\sigma} (c_{i\sigma}^\dagger c_{i\sigma} - 1), \\ \hat{\tau}(i) &= \frac{1}{2z} \sum_{j\sigma} \lambda_{ij} c_{i\sigma}^\dagger c_{j\sigma}, \\ \hat{A}(i) &= \frac{1}{2z} \sum_{j\sigma} \sigma \lambda_{ij} c_{i\sigma}^\dagger c_{j\sigma}, \\ \hat{\pi}(i) &= \frac{(-1)^i}{2z} \sum_{j\sigma} \lambda_{ij} c_{i\sigma}^\dagger c_{j,-\sigma}^\dagger, \\ \hat{\eta}(i) &= \frac{(-1)^i}{2z} \sum_{j(i),\sigma} \sigma c_{i\sigma}^\dagger c_{j,-\sigma}^\dagger, \end{aligned} \quad (24)$$

where  $j(i)$  are the nearest neighbor sites of site  $i$ . The susceptibility  $\chi_Q(0)$  is related to the isothermal compressibility  $\kappa_T$  by

$$\kappa_T = \chi_Q(0)/n^2. \quad (25)$$

The bond-charge order parameter  $\tau$  characterizes an instability towards a spontaneous deformation of the FS [42], i.e. anisotropy in  $x$  and  $y$  directions, the so called Pomeranchuk instability [14]. Analogously, a bond-spin order parameter  $A$  characterizes a spin-dependent Pomeranchuk instability. The operators  $\hat{\pi}$  and  $\hat{\eta}$  correspond to triplet and singlet pairing with momentum  $\mathbf{Q} = (\pi, \pi)$ .

Picking up the logarithmical divergences in  $\lambda$  we obtain the RG equations for the susceptibilities in the same approximations as discussed above (cf. Refs. [30,38–40])

$$d\chi_m(\lambda)/d\lambda = d_{a_m}(\lambda)\mathcal{T}_m^2(\lambda), \quad (26)$$

$$d\ln\mathcal{T}_m(\lambda)/d\lambda = d_{a_m}(\lambda)\Gamma_m(\lambda),$$

where the coefficients  $\Gamma_m$  are given by

$$\begin{aligned} \Gamma_{\text{CDW}} &= g_2 - g_3 - 2g_1; & \Gamma_{\text{SDW}} &= g_2 + g_3; \\ \Gamma_{\text{CF}} &= g_2 + g_3 - 2g_1; & \Gamma_{\text{SF}} &= g_2 - g_3; \\ \Gamma_\pi &= g_1 - g_2; & \Gamma_\eta &= -g_1 - g_2; \\ \Gamma_Q &= g_1 - 2g_2 - g_4; & \Gamma_F &= g_1 + g_4; \\ \Gamma_\tau &= -g_1 + 2g_2 - g_4; & \Gamma_A &= g_4 - g_1; \\ \Gamma_{\text{dSC}} &= g_3 - g_4. \end{aligned} \quad (27)$$

In Eqs. (26)  $a_m = 0$  for the dSC phase;  $a_m = 1$  for SDW, CDW, SF, and CF phases,  $a_m = 2$  for F, Q,  $\tau$  and  $A$  phases, and  $a_m = 3$  for  $\pi$  and  $\eta$  phases. Eqs. (26) have to be solved with the initial conditions  $\mathcal{T}_m(0) = 1$ ,  $\chi_m(0) = 0$ . At  $\lambda = 0$  the vertices (27) coincide with those considered in the mean-field approach in section II (see Eq. (5)).

Numerical solutions of Eqs. (21) show, that at a critical value  $\lambda_c$  of the scaling parameter  $\lambda$  some of the vertices and susceptibilities are divergent. We analyze the behavior of the

coupling constants  $g_1$  to  $g_4$  for  $\lambda \rightarrow \lambda_c$  representing it in the form  $(\beta_1 \dots \beta_4)$  where  $\beta_i = 0, +$  or  $-$  describes the behavior of the coupling constant  $g_i$ : the “plus” (“minus”) sign means relevant in the RG sense and tends to  $+\infty$  ( $-\infty$ ) and zero means irrelevant. To identify the leading instabilities we calculate the inverse susceptibilities for  $\lambda < \lambda^*$  ( $\lambda^*$  is the value of the scaling parameter  $\lambda$  when the largest absolute value of the coupling constants  $|g_i|$  exceeds unity) and then use a linear extrapolation of the inverse susceptibility (see Fig. 7 below). From the RG point of view, at  $\lambda \sim \lambda^*$  the “one-dimensional-like” behavior of the coupling constants considered above changes to two-dimensional and also the parts of the FS far from the van Hove points become non-negligible. However, since the values of the susceptibilities are large already at  $\lambda^*$ , the corresponding critical region is narrow.

For a given  $\lambda_c$  the size  $\Lambda$  of the patches is restricted by  $\Lambda \ll \pi$  and  $\ln(4/\Lambda) \ll \lambda_c$ . The latter criterion follows from the condition that the contribution of the electrons with  $|k_{\pm}| < \Lambda$  to particle-hole and particle-particle bubbles is dominant (see, e.g. Ref. [42]). We choose  $\Lambda = 1$  and require  $\lambda_c \gg \ln 4 \simeq 1$ . Since  $\lambda_c$  decreases with increasing interaction, this criterium restricts the values of the interactions where the two-patch RG approach is valid.

## B. Many-patch analysis

In the many-patch analysis we follow the temperature-cutoff renormalization group for one-particle irreducible (1PI) Green functions proposed recently by Honerkamp and Salmhofer in Ref. [41]. This version of the RG uses the temperature as a natural cutoff parameter, allowing to account for both the excitations with momenta close to the Fermi surface and far from it, which is necessary for the description of the particle-hole instabilities with zero momentum transfer, e.g. ferromagnetism, phase separation, and the Pomeranchuk instability. Neglecting the frequency dependence of the vertices, which is justified in the weak-coupling regime, the RG differential equation for the temperature- and momentum-dependent electron-electron interaction vertex (see the diagrammatic representation in Fig. 3), has the form

$$\begin{aligned}
\frac{d}{dT} V_T(\mathbf{k}_1, \mathbf{k}_2, \mathbf{k}_3) = & - \sum_{\mathbf{p}} V_T(\mathbf{k}_1, \mathbf{k}_2, \mathbf{p}) L_{pp}(\mathbf{p}, -\mathbf{p} + \mathbf{k}_1 + \mathbf{k}_2) V_T(\mathbf{p}, -\mathbf{p} + \mathbf{k}_1 + \mathbf{k}_2, \mathbf{k}_3) \\
& + \sum_{\mathbf{k}} [ -2V_T(\mathbf{k}_1, \mathbf{p}, \mathbf{k}_3) V_T(\mathbf{p} + \mathbf{k}_1 - \mathbf{k}_3, \mathbf{k}_2, \mathbf{p}) + V_T(\mathbf{k}_1, \mathbf{p}, \mathbf{k}_3) V_T(\mathbf{k}_2, \mathbf{p} + \mathbf{k}_1 - \mathbf{k}_3, \mathbf{p}) \\
& + V_T(\mathbf{k}_1, \mathbf{p}, \mathbf{p} + \mathbf{k}_1 - \mathbf{k}_3) V_T(\mathbf{p} + \mathbf{k}_1 - \mathbf{k}_3, \mathbf{k}_2, \mathbf{p}) ] L_{ph}(\mathbf{p}, \mathbf{p} + \mathbf{k}_1 - \mathbf{k}_3) \\
& + \sum_{\mathbf{k}} V_T(\mathbf{k}_1, \mathbf{p} + \mathbf{k}_2 - \mathbf{k}_3, \mathbf{p}) L_{ph}(\mathbf{p}, \mathbf{p} + \mathbf{k}_2 - \mathbf{k}_3) V_T(\mathbf{p}, \mathbf{k}_2, \mathbf{k}_3)
\end{aligned} \tag{28}$$

where

$$\begin{aligned}
L_{ph}(\mathbf{k}, \mathbf{k}') &= \frac{f'_T(\varepsilon_{\mathbf{k}}) - f'_T(\varepsilon_{\mathbf{k}'})}{\varepsilon_{\mathbf{k}} - \varepsilon_{\mathbf{k}'}} \\
L_{pp}(\mathbf{k}, \mathbf{k}') &= \frac{f'_T(\varepsilon_{\mathbf{k}}) + f'_T(\varepsilon_{\mathbf{k}'})}{\varepsilon_{\mathbf{k}} + \varepsilon_{\mathbf{k}'}}
\end{aligned} \tag{29}$$

and  $f'_T(\varepsilon) = df(\varepsilon)/dT$ . Eq. (28) has to be solved with the initial condition  $V_{T_0}(\mathbf{k}_1, \mathbf{k}_2, \mathbf{k}_3) = g(\mathbf{k}_1, \mathbf{k}_2, \mathbf{k}_3, \mathbf{k}_1 + \mathbf{k}_2 - \mathbf{k}_3)$  where the initial temperature  $T_0$  is of the order of the bandwidth. The evolution of the vertices with decreasing temperature determines the temperature dependence of the susceptibilities according to [41,37]

$$\begin{aligned}
\frac{d}{dT} \chi_{mT} &= \sum_{\mathbf{k}'} \mathcal{T}_{mT}(\mathbf{k}') \mathcal{T}_{mT}(\mp \mathbf{k}' + \mathbf{Q}_m) L_{pp,ph}(\mathbf{k}', \mp \mathbf{k}' + \mathbf{q}_m), \\
\frac{d}{dT} \mathcal{T}_{mT}(\mathbf{k}) &= \mp \sum_{\mathbf{k}'} \mathcal{T}_{mT}(\mathbf{k}') \Gamma_{mT}(\mathbf{k}, \mathbf{k}') L_{pp,ph}(\mathbf{k}', \mp \mathbf{k}' + \mathbf{q}_m)
\end{aligned} \tag{30}$$

where

$$\Gamma_{mT}(\mathbf{k}, \mathbf{k}') = \begin{cases} V_T(\mathbf{k}, \mathbf{k}', \mathbf{k}' + \mathbf{q}_m) - 2V_T(\mathbf{k}, \mathbf{k}', \mathbf{k} + \mathbf{q}_m) & \text{for } m = \text{CDW, CF, Q and } \tau, \\ V_T(\mathbf{k}, \mathbf{k}', \mathbf{k}' + \mathbf{q}_m) & \text{for } m = \text{SDW, SF, F, and A,} \\ V_T(\mathbf{k}, -\mathbf{k} + \mathbf{q}_m, \mathbf{k}') & \text{for } m = \pi, \eta, \text{ and dSC.} \end{cases} \tag{31}$$

$\mathbf{q}_m = \mathbf{Q}$  for CDW, SDW, CF, SF,  $\pi$  and  $\eta$ , and  $\mathbf{q}_m = \mathbf{0}$  otherwise. The upper signs in Eq. (30) refer to the particle-particle response ( $\pi, \eta$  and dSC), the lower signs to the particle-hole response. The initial conditions for Eqs. (30) are

$$\mathcal{T}_{m,T_0}(\mathbf{k}) = \begin{cases} \cos k_x - \cos k_y & \text{for CF, SF, PI, A, dSC, and } \pi, \\ 1 & \text{otherwise,} \end{cases} \tag{32}$$

and  $\chi_{m,T_0} = 0$ . To solve numerically Eqs. (28) and (30), we use the discretization of momentum space in 32 patches and the same patching scheme as proposed in Ref. [41] (we

have checked in selected cases that increasing the number of patches to 48 does not change the results). With account of the symmetries of the square lattice, this reduces the above integro-differential equations to a set of 1920 differential equations which were solved numerically. We use the value of the starting temperature  $T_0 = 12t$ , which is slightly larger than the bandwidth, and stop the flow of the coupling constants where the largest coupling constant  $V_{\max} = 18t$ . As for the two-patch analysis, we extrapolate the resulting inverse susceptibilities and calculate the critical values of the scaling parameter  $\lambda_c^m$  where the extrapolated inverse susceptibilities vanish. Due to this procedure, the results of RG analysis do not depend strongly on  $V_{\max}$ . Note that the initial  $k$ -dependence of the response functions (32) is slightly changed during the renormalization-group flow: responses with  $d$ -wave symmetry (CF, SF, PI, A, dSC, and  $\pi$ ) acquire  $g$ -wave and higher-order harmonics, while responses with  $s$ -wave symmetry acquire additional extended  $s$ -wave ( $\cos k_x + \cos k_y$ ). However, these additional corrections are small.

### C. Results of the RG analysis

For the calculations we choose the interaction strength  $U = 2t$  since for stronger interactions and moderate  $|J|/U$  and  $|V|/U$  the RG approach becomes unreliable. The phase diagrams calculated with this value of  $U$ , different values of  $t'/t = 0, 0.1, 0.3$  and the corresponding van Hove fillings are presented in Figs. 4-6. The phase boundaries, determined from the two-patch approach are shown by thin solid and dashed lines. Solid lines separate the phases with different behavior of the coupling constants, while dashed lines separate phases with the same behavior of the coupling constants and are determined from the condition of the equality of the corresponding critical values  $\lambda = \lambda_c^m$  where the linearly extrapolated susceptibilities vanish.

We consider first the results of the two-patch approach. Since this approach is applicable for not too small  $\lambda_c$  (see Section IIIA), we consider only the region of the phase diagrams with  $\lambda_c > 2$ , which is bounded by bold lines. In the most part of the phase diagrams the

typical values of  $\lambda_c$  range from 3 to 5. The dependencies of the inverse susceptibilities on the scaling parameter for selected parameter values are shown in Fig. 7. For not too large values of  $|J|$  ( $J < 0$ ) and for  $t' = 0$  or  $t' = 0.1t$  (Figs. 4,5) the two-patch approach predicts that the spin-flux phase of the type  $(0 + --)$  is the leading instability. With increasing  $V$  this phase is replaced by a phase which has comparable CDW and CF susceptibilities (CDW phase) and the behavior of the coupling constants  $(--0+)$ . With increasing  $J$  up to  $J \gtrsim 0.25U$  the CDW susceptibility dominates but also  $\chi_\tau$  and  $\chi_{SF}$  are large (we term this phase CDW'). The corresponding flow of the coupling constants is  $(0 + --)$ . At large negative  $V$  a phase of type  $(0 - 0-)$  occurs where the largest diverging susceptibility is  $\chi_Q$  which, according to Eq. (25), implies a divergent isothermal compressibility  $\kappa_T$ . A divergence of  $\kappa_T$  can be attributed generally to different phenomena: a metal-insulator transition [46] or phase separation. In the considered parameter region the most natural explanation is phase separation induced by a large negative  $V$ . For large enough  $|J|$  ( $J < 0$ ) we obtain the ferromagnetic state (F) with the coupling constant flow  $(++0+)$ ; for large positive  $V$   $\chi_A$  is the most diverging susceptibility. However, for small  $t' \lesssim 0.3t$  these instabilities are outside of the weak-coupling region of the phase diagram. The dashed area corresponds to the frustrated regime where the critical value of the scaling parameter  $\lambda_c > 20$  and the spin-density-wave instability is strongly suppressed by negative  $J$ . Such behavior arises from the competition between antiferromagnetic and superconducting fluctuations on one side and ferromagnetic fluctuations on the other side. As a result different types of instabilities almost “cancel” each other.

Four other phases (SDW, dSC, CF and PI) have the same flow of the coupling constants  $(0 + + -)$ . The magnitudes of the susceptibilities  $\chi_{dSC}$ ,  $\chi_{SDW}$ ,  $\chi_{CF}$  in the region  $J > 0$  are close to each other (see Fig. 7b), which naturally implies a close competition between these states. With increasing  $J$  we find a PI phase where the susceptibility  $\chi_\tau$  is largest. However, this instability also always appears outside of the weak-coupling region of the phase diagram where the equations (21) are valid.

As in the mean-field solution, away from half filling one expects phase separation or

the formation of inhomogeneous structures of all ordered phases with wavevector  $\mathbf{Q}$  (CDW, SDW, CF and SF). Note however, that this filling-induced type of phase separation should be contrasted with the interaction-induced phase separation in the PS region of the phase diagram, which is present even at half-filling ( $t' = 0$ ) and may not be magnetically ordered or superconducting.

The results of the many-patch approach are shown by different symbols, explained in the figure captions. Solid symbols correspond to different types of ordering tendencies. Open symbols correspond to frustrated behavior, where the many-patch RG could not reach  $V_{\max} = 18t$  for  $\lambda_T = \ln(t/T)/2 < 4$ . Boundaries between some phases (e.g. CDW and SF, dSC and PS for  $J > 0$ ) almost coincide in the two- and many-patch approaches. At the same time, the many-patch approach predicts a much broader region of stability for the SDW phase and an almost vanishing region of stability for the CF phase. Therefore, for  $t' = 0$  and  $t' = 0.1$  taking into account more patches on the FS (and therefore the contribution of nested parts) moves the predicted phase boundaries closer to those of the mean-field results. At the same time, the charge flux, as well as the  $d$ -wave superconducting response in the many-patch approach are substantial within the antiferromagnetic phase, which implies a close competition between the above ordering tendencies. For a rough estimate, where the charge response is closest to the antiferromagnetic one, we bound the region with  $\chi_{\text{CF}} > (2/3)\chi_{\text{SDW}}$  by thin crosses.

At  $J < 0$  many-patch approach does confirm the possibility of a spin flux phase in almost the same parameter region as determined from the two-patch approach. With decreasing  $V$  this spin flux phase is however replaced by a (partially frustrated) ferromagnetic phase, which fills most of the region where the frustrated SDW order was expected in the two-patch approach. The presence of the ferromagnetic phase at  $J < 0$  resembles closeby the mean-field prediction in this parameter range. The  $d$ -wave superconducting region for  $J < 0$  is replaced by phase separation in the many-patch approach.

Note that with decreasing of  $U$  the region of  $d$ -wave superconductivity at  $J > 0$  grows, while increasing of  $U$  favors the SDW instability at  $J > 0$ . Similarly, at  $J < 0$  decreasing  $U$

shifts the balance between SF phase and ferromagnetism towards the spin-flux phase. Other phases (e.g. CDW and PS) are essentially not influenced by varying  $U$ .

When increasing  $t'$  up to  $t' = 0.3t$  the phase diagram changes (see Fig. 6). In the two-patch approach, at  $J > 0.05U$   $d$ -wave superconductivity becomes the leading instability. For large positive  $V$  we obtain either CDW and A instabilities (CDW phase on Fig. 6) or CDW and PI instabilities (CDW' phase) depending on  $J$ . For large negative  $V$  we again find interaction-induced phase separation. Most of the region with  $J < 0.05U$  and moderate  $|V|$  is frustrated ( $\lambda_c > 20$ ), which is again the result of a strong competition of different ordering tendencies.

The many-patch approach also gives the strongest tendency to  $d$ -wave superconductivity at  $J > 0.05U$ , but the tendency towards ferromagnetic order in a large part of the frustrated region  $J < 0.05U$ . Similar to  $t' = 0$  and  $t' = 0.1t$ , at  $t' = 0.3t$ , the  $d$ -wave superconducting region for  $J < 0$  predicted by the two-patch approach is replaced by phase separation in the many-patch approach. The boundary of the CDW phase also almost coincides for the many-patch and two-patch approach. Therefore, at  $t' = 0.3t$  the predictions of the two-patch approach are closer to the results of the many-patch approach, than for smaller  $t'$ . This is connected with the absence of nested parts of the Fermi surface, as discussed above.

In summary, the RG analysis gives a much richer phase diagram than anticipated from the mean-field results of the previous section. At the same time, for small  $t'$  the results of the many-patch RG approach, which takes into account the contributions of the whole FS and therefore treats the renormalization of the interactions in a more accurate way, are closer to the mean-field predictions than the results of the two-patch approach. At intermediate  $t'$  the two-patch approach becomes more reliable and the results of both approaches are close. In the next section we supplement the above RG studies by an  $SO(8)$  symmetry analysis.

#### IV. SYMMETRIES AND ASYMPTOTIC BEHAVIOR

Additional insight to the phase diagram is obtained by considering the symmetries of the Hamiltonian (1) with respect to the  $SO(8)$  symmetry group of transformations of the 4-fermion states  $|\mathbf{k} \uparrow\rangle, |\mathbf{k} \downarrow\rangle, |\mathbf{k} + \mathbf{Q} \uparrow\rangle$  and  $|\mathbf{k} + \mathbf{Q} \downarrow\rangle$  (see e.g. Ref. [49]). This group is generated by the  $so(8)$  algebra of 28 operators which are given in part by

$$\hat{O}_m = \frac{1}{N} \sum_i \hat{O}_m(i) \quad (33)$$

with  $\hat{O}_m(i)$  as defined above in Eqs. (2) and (24). For a full list of operators of the  $so(8)$  algebra we refer to Ref. [49]. From the operators  $\hat{O}_m$  of the  $so(8)$  algebra we construct the rotation operators

$$R_m(\alpha) = \exp(i\alpha \hat{O}_m^\dagger + i\alpha \hat{O}_m) \quad (34)$$

where  $\alpha$  is a real number. From the symmetry point of view, the operators  $\hat{O}_m = \hat{\pi}, \hat{\eta}, \hat{A}$ , and  $\hat{\tau}$  are most useful. As discussed in Refs. [49,21], the operator  $R_\pi$  performs a rotation between SDW and dSC states (which is the basis of the  $SO(5)$  theory [1]), the operator  $R_\eta$  between dSC and CF states, the operator  $R_A$  between SDW and CF phases as well as CDW and SF phases while the operator  $R_\tau$  rotates between SDW and SF phases and between CDW and CF phases, respectively.

The symmetry of the Hamiltonian (1) under these operations is as follows. The non-interacting part of the Hamiltonian is invariant ( $H_0 = R_m H_0 R_m^{-1}$ ) under the rotations  $R_A$  and  $R_\tau$  and in the nesting case  $\varepsilon_{\mathbf{k}} = -\varepsilon_{\mathbf{k}+\mathbf{Q}}$  under  $R_\pi$  and  $R_\eta$ . The interaction is invariant only under the rotations  $R_\eta$  for  $V = J = 0$ , i.e. the Hubbard model, which was originally discovered by Yang and Zhang [50] but the interaction is not invariant with respect to the other rotation operations.

The symmetry of the restricted two-patch Hamiltonian (16) is considerably higher [42]. For this restricted Hamiltonian the interaction part, and therefore the entire Hamiltonian at half-filling and zero  $t'$ , is invariant with respect to the operations  $R_\pi, R_\eta, R_A$  or  $R_\tau$  on

special lines in the  $V$ - $J$  plane (at fixed  $U$ ). The corresponding lines are supplied by captions in Fig. 4, corresponding to the type of the symmetry. The symmetry lines exactly coincide with the boundaries between different phases in the two-patch approach, since the corresponding susceptibilities  $\chi_m(\lambda)$  in this approach are identical on these lines for arbitrary  $\lambda$ . At the same time, as we have seen in Section III, most of these symmetries (those which are connected with the SDW order) are broken by the contribution of the nested parts of FS. Away from half-filling or at finite  $t'$  the non-interacting part of the Hamiltonian becomes invariant only with respect to the rotations  $R_A$  and  $R_\tau$ .

To get more insight into the possibility of different ordering tendencies, we rewrite the Hamiltonian in terms of the operators of the  $so(8)$  algebra. We restrict ourselves to the contribution of the vH points, since the corresponding analysis for the whole FS becomes very complicated and requires numerical diagonalization of the corresponding Hamiltonian. Taking into account that the non-interacting part of the Hamiltonian (16) for vH points, i.e.

$$H_0 = \varepsilon_{\mathbf{k}_A} a_{\mathbf{0},\sigma}^\dagger a_{\mathbf{0},\sigma} + \varepsilon_{\mathbf{k}_B} b_{\mathbf{0},\sigma}^\dagger b_{\mathbf{0},\sigma} \quad (35)$$

vanishes at the vH filling (where  $\varepsilon_{\mathbf{k}_A} = \varepsilon_{\mathbf{k}_B} = 0$ ), the Hamiltonian is rewritten as

$$\begin{aligned} H_{eff} = & g_1(\widehat{O}_{CDW}^2 - \widehat{O}_{CF}^2) + g_2(\widetilde{Q}^2 - \tau^2) + g_3(\widehat{O}_{CDW}^2 + \widehat{O}_{CF}^2) \\ & + g_4(\widetilde{Q}^2 + \tau^2) - 2\widetilde{Q}(g_2 + g_4) \end{aligned} \quad (36)$$

where  $\widetilde{Q} = \widehat{Q} + 1/2$  and  $g_1 \dots g_4$  are the vertices determined in the two-patch approach (Sect. IIIA). These vertices can be also considered as those obtained from the many-patch analysis for the corresponding momenta, provided that the contribution of electrons with momenta far from the vH singularities is small, i.e.  $t'/t$  is not close to zero. Under these conditions, the Hamiltonian (36) can be considered as an effective Hamiltonian of the RG procedure in the previous section, which acts on the space of 16 states  $|s_A, s_B\rangle$  where  $s_{A,B} = 0, \uparrow, \downarrow$  or  $\uparrow\downarrow$  denotes the electron states with vH momenta  $\mathbf{k}_A$  or  $\mathbf{k}_B$ .

First we consider the eigenstates  $|m\rangle$  of the operators  $\widehat{O}_m$ , which are easily expressed in terms of the states  $|s_A, s_B\rangle$  and we obtain the expectation values of the Hamiltonian in the corresponding states as

$$E_m(\lambda) = \frac{\langle m | H_{eff} | m \rangle}{\langle m | m \rangle} = C(\lambda) - \Gamma_m(\lambda)/2 \quad (37)$$

where  $C(\lambda) = -(g_1 + 2g_2 - 2g_3 + g_4)/2$  is independent of  $m$  and  $\Gamma_m(\lambda)$  is defined in Eq. (27). Therefore the states which were identified in the two-patch approach as having the largest susceptibility (largest  $\Gamma_m(\lambda)$  for  $\lambda \rightarrow \lambda_c$ ) have also the lowest effective energy among the eigenstates  $|m\rangle$ .

For  $m \neq F$  or  $Q$  the eigenstates  $|m\rangle$  of the operators  $\hat{O}_m$  are not the eigenstates of the effective Hamiltonian (36), since the operators  $\hat{O}_m$  generally do not commute with this Hamiltonian. To find the eigenstates of the Hamiltonian, we represent it as a matrix with respect to the states  $|s_A, s_B\rangle$  and diagonalize it. In fact, the subspaces with even (odd) number of particles

$$N_{VH} = \langle a_{\mathbf{0},\sigma}^\dagger a_{\mathbf{0},\sigma} + b_{\mathbf{0},\sigma}^\dagger b_{\mathbf{0},\sigma} \rangle \quad (38)$$

are not mixed by the operators of the  $so(8)$  algebra and we can consider them separately. In the following, we focus on the even subspace where the interaction part of the Hamiltonian is non-trivial. The resulting energy levels and the eigenfunctions are presented in Table 1. The states  $|V_i\rangle$  are the triplet of eigenvectors of the operator  $\hat{O}_F$  with eigenvalues 1, 0 and  $-1$ , respectively. From the states  $|U_i\rangle$  one can form a doublet of vectors  $|U_1\rangle \pm |U_2\rangle$  which are the eigenvectors of the operator  $\hat{Q}$  with eigenvalues  $\mp 1$ . The other states are not eigenvectors of any operator in Eqs. (2) and (24). Considering the flow of the energy levels of the respective states which are given as a function of the coupling constants  $g_i$  in the second column of Table 1, we obtain the correspondence between the lowest energy eigenstates of the effective Hamiltonian in the two-patch RG procedure and the phases identified in Sect. III. We find that in the F and SF phases the triplet  $|V_i\rangle$  has the lowest energy. It is natural to associate the states  $|V_{1,3}\rangle$ , which have eigenvalues  $\pm 1$  of the operator  $\hat{O}_F$ , with the ferromagnetic phase and the state  $|V_2\rangle$  with the SF phase. Similarly, in the PS phase the states  $|U_i\rangle$ , in the CDW and A phases the state  $|C_1\rangle$ , and in the CDW' phase the state  $|C_2\rangle$  have the lowest energies. Finally, the  $|W\rangle$  state is common for SDW, CF, dSC, and PI instabilities, i.e. phases which

have the coupling constants flow of  $(0+++)$  type. The resulting correspondence is presented in the right column of Table 1.

To clarify possible types of orders which correspond to the eigenstates  $|k\rangle$  of the effective Hamiltonian (36), we expand these eigenstates in terms of the eigenvectors  $|m\rangle$  of the operators  $\widehat{O}_m$  by calculating the scalar products  $C_{mk} = \langle k|m \rangle$  listed in Table 2. Generally the states  $|k\rangle$  are a mixture of the states which correspond to different order parameters. So, the state  $|C_1\rangle$  in Table 1, which was identified above with CDW and A phases, mixes CDW, CF, A, and  $\eta$  types of order. The state  $|C_2\rangle$  (identified with the CDW' phase) mixes CDW, PI, and SF types of order. The state  $|U_2\rangle$  which is connected with the PS phase is also a mixture of dSC and  $\eta$  pairing. Finally the  $|W\rangle$  state mixes SDW, dSC, CF, and PI types of order in complete agreement with the results for the susceptibilities in the two-patch approach.

Although we do not analyze in this section the contribution of the whole FS, one can expect that general features learned from the simple two-patch analysis hold in this case too. Namely, we expect that the eigenstates of the whole Hamiltonian do not coincide with the eigenstates of operators, corresponding to different order parameters. Although the eigenvectors of the effective Hamiltonian corresponding to the contribution of the whole FS have a much more complicated form, we expect that the combinations of the order parameters listed in Table 2 which belong to the *same* eigenstate remain unchanged. This can be also seen from the analysis of simultaneously diverging susceptibilities in the many-patch approach. At the same time, one can not safely argue whether or not the discussed states support the coexistence of long-range orders, or whether part of the abovementioned orders are only short-range. Resolving these possibilities requires a strong-coupling analysis of the problem which is beyond the validity of one-loop renormalization-group approach.

## V. SUMMARY AND CONCLUSIONS

We considered the phase diagrams of the extended  $U$ - $V$ - $J$  Hubbard model within mean-field approximation and from RG approaches. The extended Hubbard model has a very complex phase diagram with various types of orders. The mean-field approximation provides only a rough phase diagram of the system. At positive  $J$  it leads mainly to the coexistence of antiferromagnetism with a small amplitude of  $d$ -wave superconductivity. At negative  $J$  mean-field theory predicts ferromagnetic order. For large enough positive  $V$  these phases are replaced by CDW order, while for large negative  $V$  the ground state is a  $d$ -wave superconductor. Charge- and spin- flux phases, as well as their coexistence with  $d$ -wave superconductivity are never energetically stable within the mean-field approximation.

The RG analyses at van Hove band fillings leads to substantially reacher phase diagrams (Figs. 4-6). Instabilities towards SDW, CDW, dSC, CF, SF, F order are possible in different parameter regimes. Importantly, for  $J \geq 0$  and not too large  $|V|$  SDW, CF, dSC orders have comparable susceptibilities, which signals their close competition in this parameter region. At the same time, the tendency towards the formation of charge-flux is greatly suppressed in the many-patch approach in comparison with the two-patch results, and it becomes the leading instability only in the restricted parameter range. With increasing  $|t'|$  the  $d$ -wave superconducting state becomes more preferable. Tendencies towards both spin-independent and spin-dependent Pomeranchuk instabilities are outside of the weak-coupling region of the phase diagrams where the RG analysis is applicable.

The symmetry analysis shows that most of the phases obtained within the RG approach are in fact a mixture of long- or short-range orders of different types. Resolving between short- and long-range orders for these phases requires a strong-coupling analysis of the problem which can not be performed within the RG approach.

Comparing the obtained results with the phase diagram of the 1D version of the  $U$ - $V$ - $J$  Hubbard model [18], we observe that the phase diagram of 1D model is similar to the results of the two-patch approach at half-filling. Charge- and spin-flux phases replace the staggered

bond-order-wave phase of the 1D model. The CDW, CDW' phases appear in two dimensions in the same parameter region as the CDW phase in the 1D case. For  $J > 0$  the SDW phase of the 1D system is partially substituted by  $d$ -wave superconductivity. At the same time, the results of two-patch approach are strongly changed at half filling by the contribution of the whole Fermi surface and become closer to the mean-field phase diagram, rather than to 1D results.

The physically most relevant regime of the 2D  $U-V-J$  Hubbard model is contained in the parameter range  $0 < V < U/4$ ,  $0 < J < U/2$ . The corresponding areas are shaded in Figs. 4-6. With decreasing van Hove filling we observe the following qualitative changes in the shaded area of the phase diagram: at half-filling SDW order dominates. For small doping  $\delta = 1 - n_{VH} = 0.08$ , we encounter a very complicated situation, in which SDW, charge-flux and  $d$ -wave superconductivity ordering tendencies are all simultaneously strong, although SDW order still dominates. In this regime the ground state structure is very sensitive to small parameter changes leading to a variety of possible phase transitions and the possibility for coexisting phases. Finally, at larger doping  $\delta = 0.28$  the picture becomes simpler again and only  $d$ -wave superconductivity becomes the leading instability.

Under the abovementioned circumstances of strong competition of different order parameters, the self-energy effects which are not accounted for in the one-loop RG approach can become crucial. Therefore, for a final conclusion about the possibility of a charge-flux phase in a broad parameter range of the one-band  $U-V-J$  model, the analysis of the two-loop contributions to the RG schemes remains to be performed. Another topic for future work will be to investigate to what extent the results for the one-band model  $U - V - J$  model in a specific parameter range allow implications for the competing orders in cuprate materials.

## VI. ACKNOWLEDGEMENTS

We are grateful to G. I. Japaridze, T. M. Rice, W. Metzner, and B. Binz for valuable discussions and M. Vojta for important comments. This work was supported by the Deutsche

Forschungsgemeinschaft through SFB 484.

## REFERENCES

- [1] E. Demler and S.-C. Zhang, Phys. Rev. Lett. **75**, 4126 (1995); S.-C. Zhang, Science **275**, 1089 (1997).
- [2] J.M. Tranquada, B.J. Sternlieb, J.D. Axe, Y. Nakamura, and S. Uchida, Nature **375**, 561 (1995); J.M. Tranquada, J.D. Axe, N. Ichikawa, Y. Nakamura, and S. Uchida, Phys. Rev. Lett. **54**, 7489 (1996).
- [3] J. Zaanen, Nature **404**, 714 (2000).
- [4] B. Büchner, M. Breuer, A. Freimuth, and A. Kampf, Phys. Rev. Lett. **73**, 1841 (1994).
- [5] B.I. Halperin and T.M. Rice, Solid State Phys. **21**, 115 (1968).
- [6] A.A. Nersesyan and G.E. Vacnadze, J. Low Temp. Phys. **77**, 293 (1989).
- [7] I. Affleck and J.B. Marston, Phys. Rev. B **37**, 3774 (1988).
- [8] A.A. Nersesyan, G.I. Japaridze, and I.G. Kimeridze, J. Phys. Cond. Matt. **3**, 3353 (1991).
- [9] A.F. Andreev and I.A. Grischuk, Zh. Eksp. Theor. Phys. **87**, 467 (1984) [Sov. Phys. JETP **60**, 267 (1984)].
- [10] P. Chandra, P. Coleman, and A.I. Larkin, J. Phys. Cond. Matt. **2**, 7933 (1990); P. Chandra and P. Coleman, Phys. Rev. Lett. **66**, 100 (1991).
- [11] S. Chakravarty, R.B. Laughlin, D.K. Morr, and C. Nayak, Phys. Rev. B **63**, 094503 (2001).
- [12] C.M. Varma, Phys. Rev. B **55**, 14554 (1997); Phys. Rev. Lett. **83**, 3538 (1999).
- [13] C. Nayak, Phys. Rev. B **62**, 4880 (2000); S. Tewargi, H.-Y. Kee, C. Nayak, and S. Chakravarty, ibid. **64**, 224516 (2001); S. Chakravarty, H.-Y. Kee, and C. Nayak, Int. J. Mod. Phys. B **15**, 2901 (2001).

[14] C. Halboth and W. Metzner, Phys. Rev. Lett. **85**, 5162 (2000).

[15] A. Kaminski, S. Rosenkranz, H.M. Fretwell, J.C. Campuzano, Z. Li, H. Raffy, W.G. Cullen, H. You, C.G. Olson, C.M. Varma, and H. Höchst, Nature **416**, 610 (2002).

[16] H. A. Mook, P. Dai, and F. Dogan, Phys. Rev. B **64**, 012502 (2001); H. A. Mook, P. Dai, S. M. Hayden, A. Hiess, J. W. Lynn, S.-H. Lee, and F. Dogan, Phys. Rev. B **66**, 144513 (2002).

[17] J. Voit, Phys. Rev. B **45**, 4027 (1992); G.I. Japaridze and A.P. Kampf, ibid. **59**, 12822 (1999).

[18] G.I. Japaridze (unpublished notes, private communication).

[19] A.A. Nersesyan, Phys. Lett. A **153**, 49 (1991); H.J. Schulz, Phys. Rev. B **53**, R2959 (1996); H.-H. Lin, L. Balents, and M.P.A. Fisher, ibid. **58**, 1794 (1998); J.O. Fjærstad and J.B. Marston, Phys. Rev. B **65**, 125106 (2002).

[20] X.-Z. Yan, Phys. Rev. B **48**, 7140 (1993); E. Dagotto, J. Riera, Y. C. Chen, A. Moreo, A. Nazarenko, F. Alcaraz, and F. Ortolani, ibid. **49**, 3548 (1994); B. Chatopadhyay and D.M. Gaitonde, ibid. **55**, 15364 (1997).

[21] M. Murakami, J. Phys. Soc. Jpn. **69**, 1113 (2000).

[22] A.B. Eriksson, T. Einarsson, and S. Ostlund, Phys. Rev. B **52**, 3662 (1995).

[23] M. Inui, S. Doniach, P.J. Hirschfeld, and A.E. Ruckenstein, Phys. Rev. B **37**, 2320 (1988); M. Murakami and H. Fukuyama, J. Phys. Soc. Jpn **67**, 2784 (1998), B. Kyung, Phys. Rev. B **62**, 9083 (2000).

[24] J.-X. Zhu, W. Kim, C.S. Ting, and J.P. Carbotte, Phys. Rev. Lett. **87**, 197001 (2001); C. Wu and W. V. Liu, Phys. Rev. B **66**, 020511(R) (2002)..

[25] C. Nayak and E. Pivovarov, Phys. Rev. B **66**, 064508 (2002).

[26] A.I. Lichtenstein and M.I. Katsnelson, Phys. Rev. B **62**, R9283 (2000).

[27] A. Ino, C. Kim, M. Nakamura, T. Yoshida, T. Mizokawa, A. Fujimori, Z.-X. Shen, T. Kakeshita, H. Eisaki, and S. Uchida, Phys. Rev. B **65**, 094504 (2002).

[28] P.V. Bogdanov, A. Lanzara, X.J. Zhou, S.A. Kellar, D.L. Feng, E.D. Lu, H. Eisaki, J.-I. Shimoyama, K. Kishio, Z. Hussain, and Z. X. Shen, Phys. Rev. B **64**, 180505 (2001).

[29] D.L. Feng, C. Kim, H. Eisaki, D.H. Lu, A. Damascelli, K.M. Shen, F. Ronning, N.P. Armitage, N. Kaneko, M. Greven, J. Shimoyama, K. Kishio, R. Yoshizaki, G.D. Gu, and Z.-X. Shen, Phys. Rev. B **65**, 220501(R) (2002).

[30] H.J. Schulz, Phys. Rev. B **39**, 2940 (1989).

[31] I.E. Dzyaloshinskii, Zh. Eksp. Teor. Fiz. **93**, 1487 (1987) [Sov. Phys. JETP **66**, 848 (1987)].

[32] I.E. Dzyaloshinskii and V.M. Yakovenko, Zh. Eksp. Teor. Fiz. **94**, 344 (1988) [Sov. Phys. JETP **67**, 844 (1988)]; Int. J. Mod. Phys. B **2**, 667 (1988).

[33] A.T. Zheleznyak, V.M. Yakovenko, and I.E. Dzyaloshinskii, Phys. Rev. B **55**, 3200 (1997).

[34] D. Zanchi and H.J. Schulz, Phys. Rev. B **54**, 9509 (1996); ibid. **61**, 13609 (2000).

[35] C.J. Halboth and W. Metzner, Phys. Rev. B **61**, 7364 (2000).

[36] C. Honerkamp, M. Salmhofer, N. Furukawa, and T.M. Rice, Phys. Rev. B **63**, 035109 (2001).

[37] C. Honerkamp, M. Salmhofer, and T.M. Rice, Eur. Phys. J. B **27**, 127 (2002).

[38] P. Lederer, G. Montambaux, and D. Poilblanc, J. Phys. (Paris) **48**, 1613 (1987).

[39] N. Furukawa, T. M. Rice, and M. Salmhofer, Phys. Rev. Lett. **81**, 3195 (1998).

[40] V.Yu. Irkhin, A.A. Katanin, and M. I. Katsnelson, Phys. Rev. B **64**, 165107 (2001).

- [41] C. Honerkamp and M. Salmhofer, Phys. Rev. B **64**, 184516 (2001).
- [42] B. Binz, D. Baeriswyl, and B. Doucot, Eur. Phys. J. B **25**, 69 (2002); B. Binz, PhD Thesis, University of Fribourg, 2002, (unpublished); cond-mat/0207067 (unpublished).
- [43] P.G.J. van Dongen, Phys. Rev. B **54**, 1584 (1996).
- [44] F. Guinea, G. Gomez-Santos, and D.P. Arovas, Phys. Rev. B **62**, 391 (2000).
- [45] A.A. Katanin and A.P. Kampf, unpublished.
- [46] N. Furukawa and M. Imada, J. Phys. Soc. Jpn. **61**, 3331 (1992).
- [47] M. Fleck, A. Oles, and L. Hedin, Phys. Rev. B **56**, 3159 (1997).
- [48] R. Hlubina, S. Sorella, and F. Guinea, Phys. Rev. Lett. **78**, 1343 (1997).
- [49] R.S. Markiewicz and M.T. Vaughn, J. Phys. Chem. Solids **59**, 1737 (1998); Phys. Rev. B **57**, R14052 (1998).
- [50] C.N. Yang and S.-C. Zhang, Mod. Phys. Lett. B **4**, 759 (1990).

TABLES

$k$	$E_k(\{g_i\})$	State	Corresp. phases
1.	$-g_2 - g_4$	$ V_1\rangle =  \uparrow, \uparrow\rangle,  V_2\rangle =  \uparrow, \downarrow\rangle +  \downarrow, \uparrow\rangle,  V_3\rangle =  \downarrow, \downarrow\rangle$	F, SF
2.	0	$ U_1\rangle =  0, 0\rangle +  \uparrow\downarrow, \uparrow\downarrow\rangle;  U_2\rangle =  0, 0\rangle -  \uparrow\downarrow, \uparrow\downarrow\rangle$	PS
3.	$2g_1 - g_2 - g_4$	$ C_1\rangle =  \uparrow, \downarrow\rangle -  \downarrow, \uparrow\rangle$	CDW, A
4.	$g_1 - 2g_2 + g_3$	$ C_2\rangle =  \uparrow\downarrow, 0\rangle +  0, \uparrow\downarrow\rangle$	CDW'
5.	$g_1 - 2g_2 - g_3$	$ W\rangle = - \uparrow\downarrow, 0\rangle +  0, \uparrow\downarrow\rangle$	SDW, CF, dSC, PI

Table 1. The eigenvalues  $E_k(\{g_i\})$  and eigenstates  $|k\rangle$  of the effective Hamiltonian, Eq. (36). The right column represents the correspondence with the phases in the phase diagrams (see text).

State	$ \text{SDW}\rangle$	$ \text{dSC}\rangle$	$ \text{CF}\rangle$	$ \text{SF}\rangle$	$ \text{CDW}\rangle$	$ \tau\rangle$	$ A\rangle$	$ \eta\rangle$
$\langle V_2  $	$1/\sqrt{2}$	0	0	$i/\sqrt{2}$	0	0	$1/\sqrt{2}$	0
$\langle C_1  $	0	0	$-i/\sqrt{2}$	0	$-1/\sqrt{2}$	0	$-1/\sqrt{2}$	$-1/\sqrt{2}$
$\langle C_2  $	0	0	0	$1/\sqrt{2}$	$1/\sqrt{2}$	$1/\sqrt{2}$	0	0
$\langle U_2  $	0	$-1/\sqrt{2}$	0	0	0	0	0	$-1/\sqrt{2}$
$\langle W  $	$1/\sqrt{2}$	$-1/\sqrt{2}$	$1/\sqrt{2}$	0	0	$-1/\sqrt{2}$	0	0

Table 2. The scalar products  $C_{mk} = \langle k|m\rangle$  between the eigenstates of the effective Hamiltonian, Eq. (36) (see also Table 1) and the eigenstates of the operators in Eqs. (2) and (24).

## FIGURE CAPTIONS

Fig. 1. The mean-field phase diagram for  $U = 4t$ ,  $t'/t = 0.1$  and van Hove band filling  $n = 0.92$ . SDW and CDW denote the spin- and charge-density wave phases, dSC the  $d$ -wave superconducting phase, SDW+dSC marks phase coexistence, and F is the ferromagnetic phase. Solid and dashed lines correspond to first and second order transitions, respectively.

Fig. 2. The Fermi surface at van Hove band fillings:  $t' = 0$  and  $n = 1$  (solid line),  $t'/t = 0.1$  and  $n = 0.92$  (long-dashed line), and  $t'/t = 0.3$  and  $n = 0.72$  (short-dashed line), A and B are van Hove points.

Fig. 3. Diagrammatic representation for the many-patch RG equations, Eq. (28). Lines drawn through the vertices show the direction of spin conservation. Diagrams are drawn in the same order as the respective terms in Eq. (28). The cutting dash at the propagator lines means the derivative with respect to  $T$  (for brevity we indicate only the derivative of one of the propagators, the same diagrams with derivatives of another propagator are included as well).

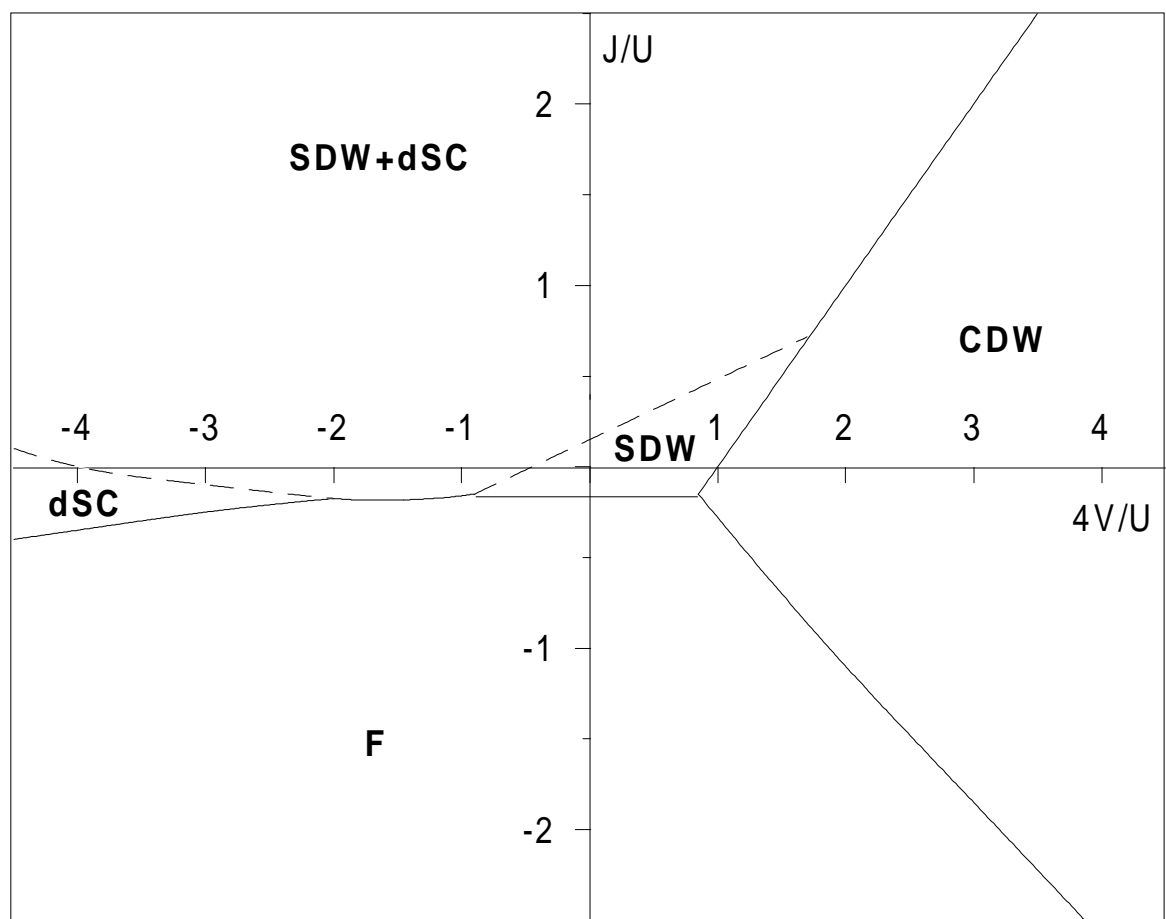
Fig. 4. Phase diagram as obtained from two- and many-patch RG analyses for  $U = 2t$ ,  $t' = 0$ , and  $n = 1$ . Bold lines bound the weak-coupling region of the phase diagram, where the RG approach is applicable. Solid lines correspond to the phase boundaries obtained from the two-patch analysis. CF and SF denote the charge- and spin-flux phases, respectively, PS is the interaction-induced phase separated state. F, PI, and A denote the possibilities for ferromagnetism (F), spontaneous spin-independent (PI) and spin-dependent (A) deformations of the FS in the corresponding strong coupling regions. The other notations are the same as in Fig.1. The shaded region is the frustrated area with the critical scaling parameter of the two-patch approach  $\lambda_c > 20$ . The captions at the phase boundary lines denote the symmetry of the Hamiltonian (16) on these lines with respect to the rotation operators  $R_\eta$ ,  $R_\pi$ ,  $R_\tau$  or  $R_A$  and the corresponding ordered states which become equivalent. The symbols correspond to the results of the many-patch RG approach: circles correspond

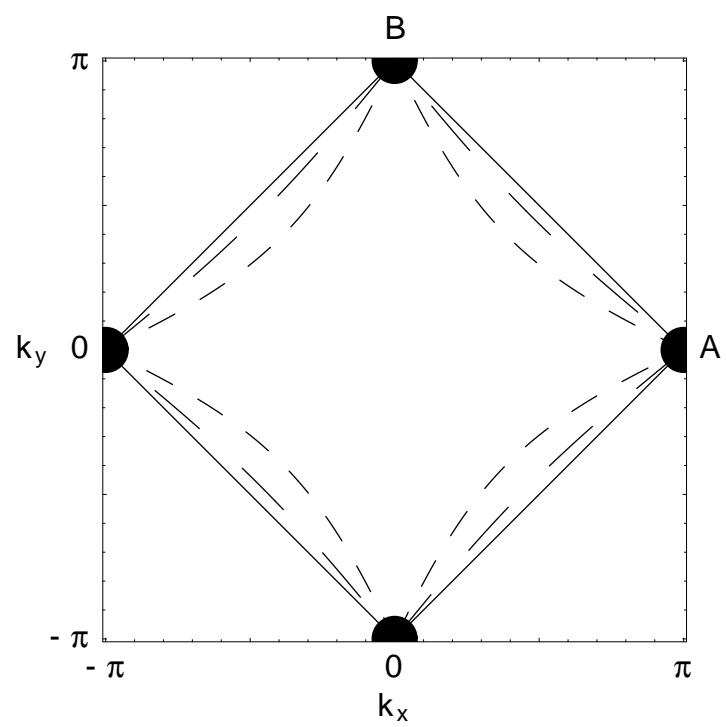
to SDW, diamonds to dSC, squares to SF, triangles to F, crosses to PS, and stars to CDW phase. The open symbols denote the frustrated regime in many-patch calculations when no divergence of the coupling constants was obtained for  $\lambda_T = \ln(t/T)/2 < 4$ . The type of the corresponding ordering tendency in this case was determined by the largest susceptibility at  $\lambda_T = 4$ .

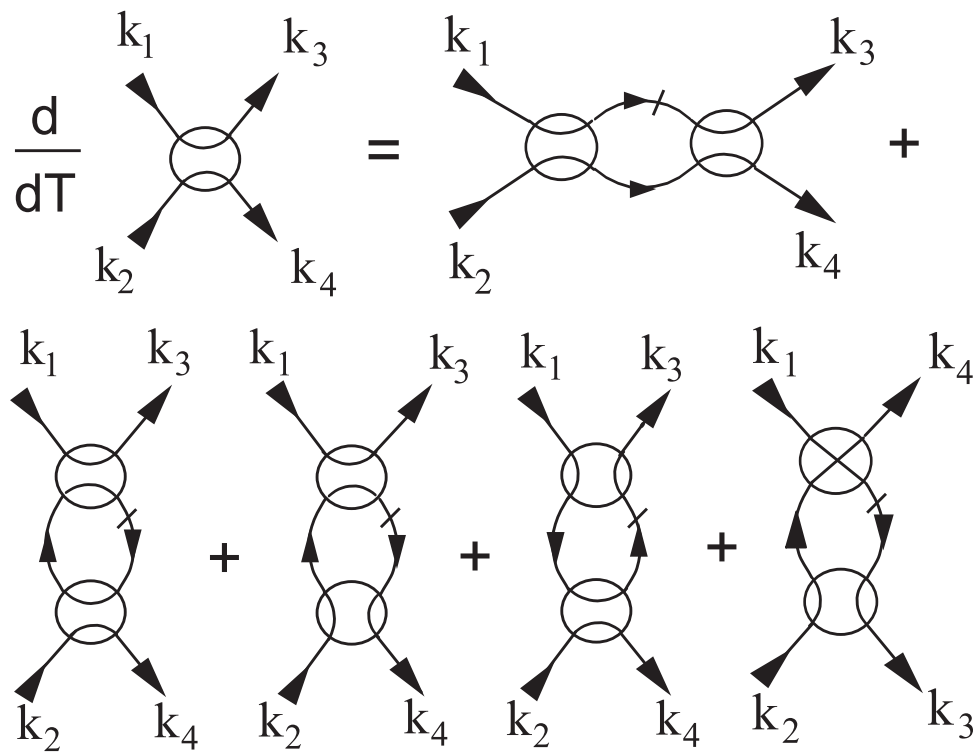
Fig. 5. Phase diagram as obtained from the RG calculations for  $U = 2t$ ,  $t'/t = 0.1$ , and  $n = 0.92$ . Solid and dashed lines correspond to the phase boundaries obtained from the two-patch analysis and separate the phases with respect to the scaling behavior of the coupling constants (see text). The half-filled circle corresponds to a charge-flux instability in the many-patch RG analysis. Thin crosses bound the bottom of the region where the charge-flux fluctuations become substantial,  $\chi_{\text{CF}} > (2/3)\chi_{\text{SDW}}$ . Other notations are the same as in Fig. 4.

Fig. 6. Phase diagram as obtained from the RG calculations for  $U = 2t$ ,  $t'/t = 0.3$ , and  $n = 0.72$ . Thin crosses bound the region where charge-flux fluctuations become substantial,  $\chi_{\text{CF}} > (2/3)\max(\chi_{\text{SDW}}, \chi_{\text{dSC}})$ . Other notations are the same as in Figs. 4,5.

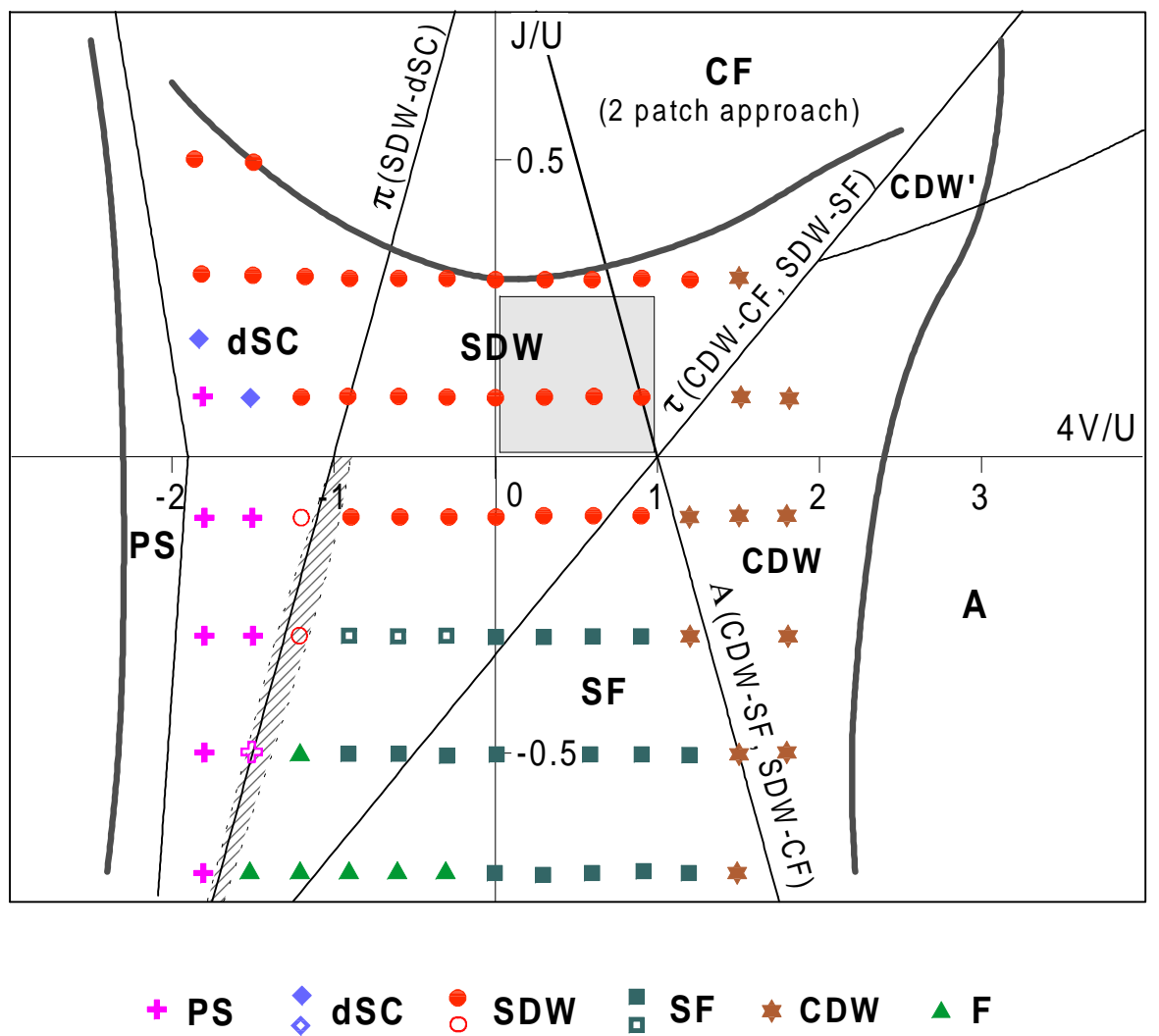
Fig. 7. Scale dependence of the leading order-parameter inverse susceptibilities in the two-patch RG approach for  $U = 2t$ ,  $t'/t = 0.1$ , and  $n = 0.92$ : a)  $V = J = 0$ ; b)  $V = 0$ ,  $J = 0.2U$ ; c)  $V = 0.5U$ ,  $J = 0$ . The vertical dot-dashed lines mark the scaling parameter  $\lambda^*$  where the largest absolute value of the coupling constants  $|g_i|$  is unity.







$t'=0.0$



$t'=0.1$

